

HS 2325 + 8205—An Ideal Laboratory for Accretion Disk Physics

S. PYRZAS,¹ B. T. GÄNSICKE,¹ J. R. THORSTENSEN,² A. AUNGWEROJWIT,^{3,4} D. BOYD,⁵ S. BRADY,⁶ J. CASARES,^{7,8}
R. D. G. HICKMAN,¹ T. R. MARSH,¹ I. MILLER,⁹ Y. ÖGMEN,¹⁰ J. PIETZ,¹¹ G. POYNER,¹²
P. RODRÍGUEZ-GIL,^{7,8} AND B. STAELS¹³

Received 2011 December 9; accepted 2012 January 30; published 2012 February 29

ABSTRACT. We identify HS 2325 + 8205 as an eclipsing, frequently outbursting, dwarf nova with an orbital period of $P_{\text{orb}} = 279.841731(5)$ minutes. Spectroscopic observations are used to derive the radial velocity curve of the secondary star from absorption features and also from the H α emission lines, originating from the accretion disk, yielding $K_{\text{sec}} = K_{\text{abs}} = 237 \pm 28$ km s $^{-1}$ and $K_{\text{em}} = 145 \pm 9$ km s $^{-1}$, respectively. The distance to the system is calculated to be 400(+200, -140) pc. A photometric monitoring campaign reveals an outburst recurrence time of ~12–14 days. The combination of magnitude range (17–14 mag), high declination, and eclipsing nature and frequency of outbursts makes HS 2325 + 8205 the ideal system for “real-time” studies of the accretion disk evolution and behavior in dwarf nova outbursts.

1. INTRODUCTION

Dwarf novae are a subclass of nonmagnetic (or weakly magnetic) cataclysmic variables (CVs; see, e.g., Warner [1995] for a comprehensive review), in which a white dwarf primary accretes matter via an accretion disk, formed by material transferred through the L_1 point from a Roche lobe-filling (near) main-sequence secondary. The defining trait of dwarf novae are quasi-periodical brightness changes of several magnitudes, commonly known as “dwarf nova outbursts.” It is widely accepted that outbursts can be understood within the framework of the disk instability model (see, e.g., Smak [1984]; Cannizzo [1993]; Osaki [1996]; Lasota [2001] for reviews of the topic).

Within the disk instability model, accretion disks undergo outbursts if the mass transfer rate is below a critical value, \dot{M}_{crit} . Above the CV orbital period gap¹⁴ accretion rates are usually larger than \dot{M}_{crit} and, as a result, only about one-third of non-magnetic systems are dwarf novae. The situation is completely different below the period gap, where dwarf novae dominate the CV population (Shafter 1992).

Dwarf novae provide the best environment to develop and test our understanding of accretion disk structure and dynamics, which is relevant to a wide range of objects, such as low-mass X-ray binaries (Dubus et al. 2001), active galactic nuclei (Burderi et al. 1998), and young stellar objects (Bell & Lin 1994).

Of particular interest in this context are eclipsing dwarf novae. In these systems, the physical properties of the binary (such as the mass ratio, the inclination angle, the masses and temperatures of the component stars, and the radial structure of the accretion disk) can be determined to high precision, through studies of the eclipse features of the white dwarf, the bright spot (formed in the region where the mass-transferring stream meets the accretion disk), and accretion disk components (see, e.g., Wood et al. 1989; Littlefair et al. 2006b; Southworth et al. 2009).

HS 2325 + 8205 (R.A.: 23^h26^m50.4^s, Dec.: +82°22'12" [J2000], henceforth HS 2325) was one of the systems identified in a dedicated search for CVs (Aungwerojwit et al. 2005) within the Hamburg Quasar Survey (Hagen et al. 1995). Photometric observations soon revealed the eclipsing nature of the system and also frequently occurring outbursts. An interesting historic note is that Morgenroth (1936) mentioned short-term variability of HS 2325, which correspondingly was included in the New

¹ Department of Physics, University of Warwick, Coventry, CV4 7AL, UK.

² Department of Physics and Astronomy, 6127 Wilder Laboratory, Dartmouth College, Hanover, NH 03755.

³ Department of Physics, Faculty of Science, Naresuan University, Phitsanulok, 65000, Thailand.

⁴ Thailand Center for Excellence in Physics, Commission on Higher Education, 328 Si Ayutthaya Road, Bangkok, 10400, Thailand.

⁵ British Astronomical Association, Variable Star Section, West Challow OX12 9TX, UK.

⁶ American Association of Variable Star Observers, 25 Birch Street, Cambridge, MA 02138.

⁷ Instituto de Astrofísica de Canarias, Vía Láctea, s/n, La Laguna, E-38205, Tenerife, Spain.

⁸ Departamento de Astrofísica, Universidad de La Laguna, E-38206 La Laguna, Tenerife, Spain.

⁹ British Astronomical Association, Variable Star Section, Furzehill House, Ilston, Swansea SA2 7LE, UK.

¹⁰ Green Island Observatory, Geçitkale, Mugosa, via Mersin 10, Cyprus.

¹¹ Nollenweg 6, 65510 Idstein, Germany.

¹² British Astronomical Association, Variable Star Section, 67 Ellerton Road, Kingstanding, Birmingham B44 0QE, UK.

¹³ Center for Backyard Astrophysics (Flanders), Alan Guth Observatory, Koningshofbaan 51, Hofstade, Aalst, Belgium.

¹⁴The orbital period range of 2 hr $\leq P_{\text{orb}} \leq$ 3 hr, where only a small number of CVs are found.

TABLE 1
LOG OF OBSERVATIONS WITH LARGE-APERTURE (>1 m) TELESCOPES

ID	Date	HJD range ^a	Telescope	Filter/grating	Exp. time (s)	Frames	Ecl.	Mag.	Depth (mag)
01	2003 Sep 05	2888.255–2888.518	KY ^b	Clear	30	646	1	14.9	0.4
02	2004 Jun 10	3167.429–3167.467	KY	Clear	30	90	0	15.1	...
03	2004 Jun 11	3168.413–3168.593	KY	Clear	30	390	1	15.7	0.8
04	2004 Jun 12	3169.451–3169.569	KY	Clear	30	270	0	16.1	...
05	2004 Jul 25	3212.455–3212.607	KY	Clear	30	389	1	16.0	0.8
06	2004 Jul 27	3214.298–3214.573	KY	Clear	30	693	2	16.2	0.8
07	2004 Oct 21	3300.212–3300.493	KY	Clear	20	997	2	16.4	0.8
08	2004 Oct 22	3301.213–3301.478	KY	Clear	20	897	1	15.9	0.7
09	2004 Oct 23	3302.214–3302.457	KY	Clear	20	858	1	14.6	0.4
10	2005 Sep 05	3619.333–3619.546	CA22 ^c	Clear	10	572	1	14.4	0.4
11	2005 Sep 11	3624.727–3624.804	HT ^d	600 lines mm ⁻¹	360/480	17
12	2005 Sep 12	3625.649–3625.909	HT	600 lines mm ⁻¹	360/480	31
13	2005 Sep 15	3629.599–3629.668	NOT ^e	Clear	4	564	1	17	0.7
14	2005 Sep 16	3630.550–3630.715	NOT	Clear	4	1308	1	16.5	0.6
15	2006 Aug 23	3971.321–3971.621	KY	Clear	30	727	1	14.5	0.4
16	2006 Oct 28	4037.248–4037.504	KY	Clear	30	595	1	16.3	0.8
17	2007 Jan 24	4124.604–4124.610	HT	600 lines mm ⁻¹	360/480	2

NOTES.—Given are the run identification number, the date of observation, the start and end of observation in HJD, the telescope, and the filter (photometry) or grating (spectroscopy) used. “Frames” denotes the number of frames collected, “Ecl” is the number of eclipses observed, “Mag” is the out-of-eclipse magnitude, and “Depth” the eclipse depth in magnitudes.

Catalogue of Suspected Variable Stars as NSV 14581 (though with rather uncertain coordinates).

2. OBSERVATIONS

We obtained photometric and spectroscopic data on HS 2325 using both large-aperture (>1 m) and small-aperture telescopes. Table 1 summarizes the observations conducted with the former. A brief account on data reduction follows.

2.1. Photometry

We obtained time-series photometry of HS 2325 during 17 nights throughout the period of 2003 to 2007 using 1.2–2.5 m telescopes (Table 1). These observations were reduced with the pipeline described in Gänsicke et al. (2004), which employs bias-subtraction and flat-fielding in the standard fashion within MIDAS and uses SExtractor (Bertin & Arnouts 1996) to perform aperture photometry. Sample light curves are shown in Figure 1.

HS 2325 has been found to vary in brightness between the ~17th and ~14th magnitudes. Eclipses are shallow and maintain an almost constant depth during the rise to outburst. The eclipses in the bright state exhibit a symmetric U shape, which is typical for an accretion-disk-dominated system. During quiescence the eclipse morphology becomes more complicated and reveals several breaks in slope. In addition to eclipses, the light curve of HS 2325 displays two further features: short-term, random, out-of-eclipse variations, known as “flickering” (e.g., Bruch 2000) and an “orbital hump,” which is a brightening just

before the start of the eclipse attributed to the bright spot coming into view (e.g., Krzeminski 1965).

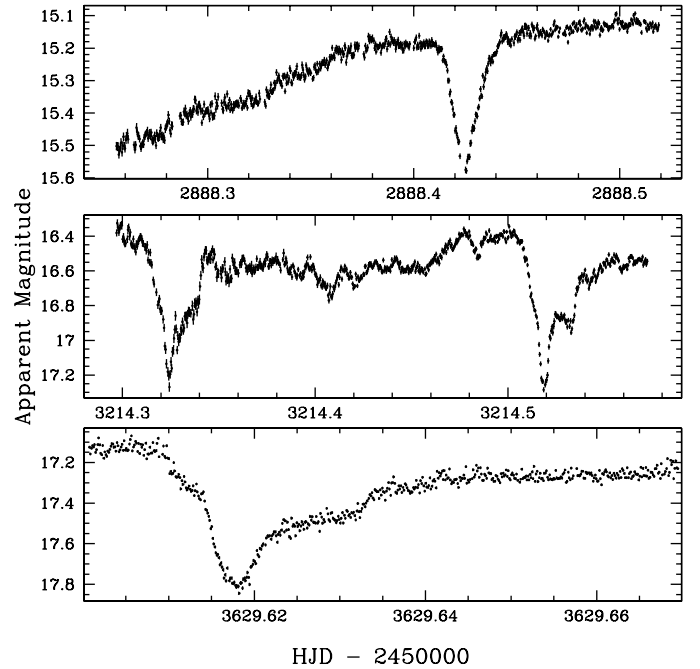


FIG. 1.—Sample light curves of HS 2325. Top: Filterless KY observations from 2003 September 5 (ID01), with the system on the rise to outburst. Middle: Filterless KY observations from 2004 July 27 (ID06), with the system in an intermediate state. Bottom: Filterless NOT observations from 2005 September 15 (ID13), with the system in quiescence.

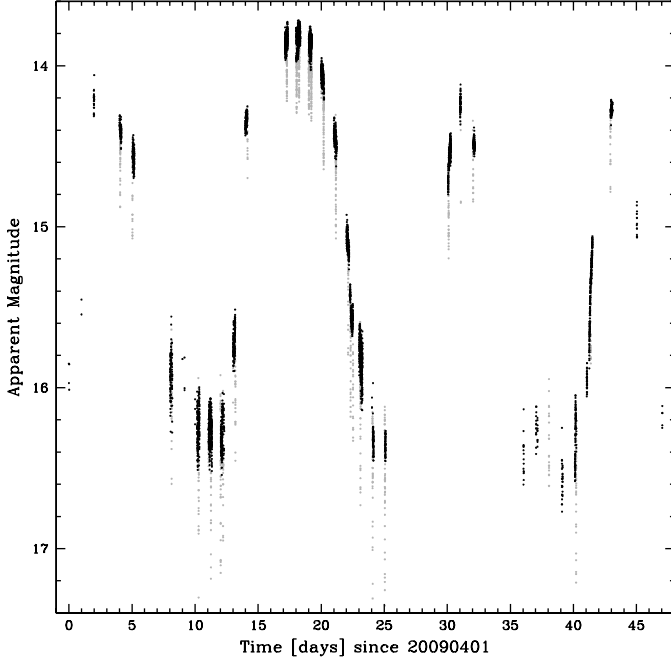


FIG. 2.—Result of the outburst monitoring campaign for HS 2325. Four outbursts have been recorded in 50 days. Points in light gray indicate the system being in eclipse.

An intensive 1.5-month-long photometric campaign was conducted in 2009 to characterize the outburst behavior of HS 2325, using small-aperture (11–14 inch) telescopes. The data were reduced with AIP4WIN and MAXIMDL, and the resulting light curve is shown in Figure 2.

2.2. Spectroscopy

Spectroscopic observations during the system's quiescence were obtained at the 2.4 m Hiltner telescope at MDM Observatory on Kitt Peak, Arizona. The modular spectrograph and a SITe 2048² pixel CCD yielded 2 Å pixel⁻¹ and from 4210 to 7500 Å, but with decreased sensitivity toward the ends of the wavelength range. The spectral resolution was ~ 3.5 Å full width at half-maximum (FWHM). Reductions were performed mostly with standard IRAF routines, but we used an original implementation of the optimal extraction algorithm detailed by Horne (1986) to compute one-dimensional spectra from the two-dimensional images. For wavelength calibration, we used a dispersion curve derived from lamp exposures in twilight, and we corrected for nighttime drifts using the $\lambda 5577$ sky-line. We observed standard stars in twilight whenever the sky appeared clear, and we used these observations to flux-calibrate the data. The scatter of the standard stars typically suggests that the flux calibration is uncertain by several tenths of a magnitude, probably due to uncalibrated losses at the spectrograph slit. The mean quiescent spectrum is shown in Figure 3. The

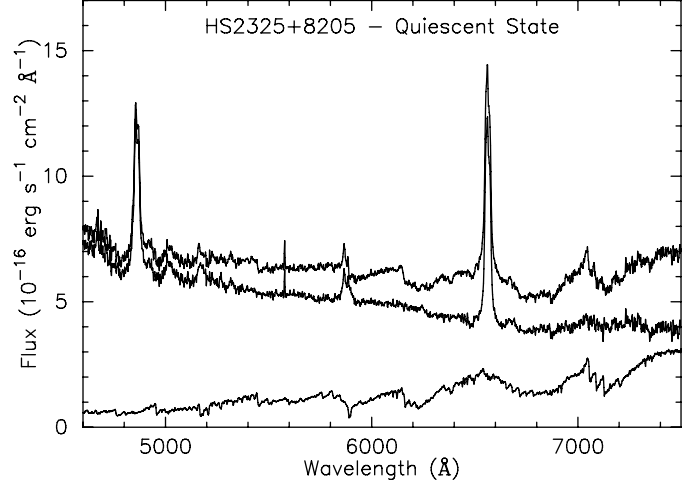


FIG. 3.—*Top trace:* Mean quiescent spectrum of HS 2325. *Middle trace:* HS 2325 spectrum minus the scaled M dwarf. *Bottom trace:* A library spectrum of the M3 dwarf Gliese 436, scaled so that it has an apparent *V*-band magnitude of ~ 19.0 .

flux level of the observed spectrum implies a *V*-band magnitude near 17.0, subject to the calibration uncertainties.

3. ORBITAL PERIOD AND EPHEMERIS

Mideclipse times (given in Table 2) were determined by visually cross-correlating each eclipse profile with its mirror image with respect to time. This was found to produce more robust results than fitting a parabola to the eclipse minimum: in particular, for the light curves with poor time resolution. We adopted the duty cycle (exposure plus readout time) of the corresponding observations as a conservative estimate of the uncertainty in the mideclipse times.

Fitting a linear ephemeris to the mideclipse times gives

$$T_0(\text{HJD}) = 2,452,888.42554(3) + 0.194334535(3) E, \quad (1)$$

with mideclipse times calculated on a UTC timescale, i.e., an orbital period of $P_{\text{orb}} = 279.841731(5)$ minutes.

4. SECONDARY SPECTRAL TYPE AND RADIAL VELOCITY ANALYSIS

As is typical for quiescent dwarf novae, the Balmer lines in emission are the most prominent features in the spectrum of HS 2325, with equivalent widths of ≈ 30 and ≈ 54 Å for H β and H α , respectively. He I emission is detected at 4921, 5015, and 5876 Å, and Fe II is detected at $\lambda 5169$ (the features at $\lambda\lambda 4921$ and 5015 may also be blended with Fe II). The absorption bands of an M dwarf companion are conspicuous. To quantify the M dwarf contribution, we subtracted library spectra of M dwarfs classified by Boeshaar (1976), taken with the same instrument, and varied the spectral type and scaling until the M dwarf features were canceled as well as possible. The lower two

TABLE 2
MIDECLIPSE TIMES

T_0 (HJD)	Error (HJD)	$O - C$ (s)	Cycle	T_0 (HJD)	Error (HJD)	$O - C$ (s)	Cycle	T_0 (HJD)	Error (HJD)	$O - C$ (s)	Cycle	
2888.425480	0.000405	-6	0	4320.476770	0.000463	3	7369	4940.598350	0.000463	10	10560
3168.461560	0.000405	-4	1441	4335.440630	0.000463	12	7446	4941.375690	0.000775	10	10564
3212.575440	0.000405	-9	1668	4358.371920	0.000463	-4	7564	4941.569840	0.000463	-6	10565
3214.324580	0.000405	2	1677	4379.360110	0.000463	1	7672	4942.347170	0.001157	-7	10569
3214.518890	0.000405	-0	1678	4393.352210	0.000463	2	7744	4942.541460	0.000463	-11	10570
3300.220510	0.000289	7	2119	4451.458200	0.000810	-1	8043	4943.513250	0.001157	-0	10575
3300.414840	0.000289	7	2120	4510.535910	0.000463	0	8347	4944.485020	0.001157	8	10580
3301.386470	0.000289	3	2125	4524.527990	0.000810	-1	8419	4945.456530	0.001157	-6	10585
3302.357990	0.000289	-10	2130	4544.544400	0.000463	-5	8522	4945.650900	0.000660	-3	10586
3619.512060	0.000231	-1	3762	4560.479940	0.000810	5	8604	4945.845190	0.000660	-7	10587
3629.617580	0.000116	10	3814	4927.383490	0.000775	0	1049	4946.428210	0.001157	-6	10590
3630.589230	0.000116	8	3819	4933.602120	0.000810	-6	1052	4947.399870	0.000775	-7	10595
3971.452040	0.000405	11	5573	4934.573920	0.000810	4	1052	4948.371720	0.000660	8	10600
4037.331340	0.000405	2	5912	4935.351320	0.000775	10	1053	4963.529620	0.000810	-8	10678
4289.577510	0.000463	-3	7210	4935.545640	0.001007	8	1053	4964.695730	0.000810	0	10684
4312.508950	0.000463	-6	7328	

NOTE.— T_0 : UTC expressed as Heliocentric JD $-2,450,000$; Error: Estimated uncertainty; $O - C$: Difference from the ephemeris of Eq. (1); Cycle: Cycle number in the ephemeris of Eq. (1).

traces in Figure 3 show the decomposition that was (at least subjectively) the best. From this exercise, we estimate that the companion is of type $M3.0 \pm 0.75$ subclasses and that its flux corresponds to $V = 19.0 \pm 0.4$ (external error, including calibration uncertainties). The spectral type-period relation of Smith & Dhillon (1998; eq. [4] in their article) for $P > 4$ hr yields $Sp2 = M1.5$ for the derived orbital period of $P_{\text{orb}} = 4.664$ hr, which is a value broadly consistent with our estimate of $M3.0 \pm 0.75$, as the rms scatter of the spectral type-period relation is three subtypes for $P > 4$ hr (Smith & Dhillon 1998).

We measured radial velocities of the $H\alpha$ emission line using a double-Gaussian convolution method outlined by Schneider & Young (1980); the centers of the Gaussians were separated by 1280 km s^{-1} , and each individual Gaussian had a FWHM of 270 km s^{-1} , comparable with our spectral resolution. This emphasized the outer wings of the line profile. We also tried a range of separations and found that the radial velocity amplitude and phase were insensitive to this parameter. To measure the velocity of the M dwarf component, we used the cross-correlation program rvsao, written by Kurtz & Mink (1998). For the template, we used a velocity-compensated composite M dwarf spectrum, composed by summing the spectra of a large number of M dwarfs for which Marcy et al. (1987) tabulate precise velocities. The cross-correlation region was from 6000 to 6500 Å; this was chosen to include some strong atomic and TiO features, while avoiding emission lines. Not all the spectra gave usable cross-correlation velocities; we limited our analysis to those for which the formal velocity error was less than 35 km s^{-1} .

We then performed fits to the radial velocities (both absorption and $H\alpha$ emission), of the form $v(t) = \gamma + K \sin[(t - T_0)/P_{\text{orb}}]$. The orbital period P_{orb} was held fixed to the value derived from

eclipses. Because of the modest number of absorption velocities and their limited phase coverage, and because the absorption should trace the motion of the secondary star fairly well, we fixed T_0 to the mideclipse ephemeris when fitting the absorption velocities, but left it as a free parameter for the $H\alpha$ emission ones. The resulting velocities were $K_{\text{sec}} = K_{\text{abs}} = 237(28) \text{ km s}^{-1}$, $\gamma_{\text{abs}} = -19(20) \text{ km s}^{-1}$, $K_{\text{em}} = 145(9) \text{ km s}^{-1}$, and $\gamma_{\text{em}} = -42(6) \text{ km s}^{-1}$ for the absorption and emission lines, respectively, with the numbers in parentheses indicating the errors. Figure 4 shows the emission and absorption velocities as a function of orbital phase, and Figure 5 shows a grayscale representation of the low-state spectra, as a function of phase. The upper panel of Figure 5 is scaled to emphasize the M dwarf absorption features and to show the structure in the He I $\lambda 5876$ line; the orbital motion of the M dwarf is clearly seen. The scaling of the lower panel brings out the complex structure in the $H\alpha$ emission.

5. DISTANCE

We can estimate the distance to HS 2325 using the secondary star's contribution to the spectrum and our knowledge of the orbital period P_{orb} . For a secondary star of mass M_{sec} at a fixed P_{orb} , the Roche lobe radius R_2 is proportional to $M_{\text{sec}}^{1/3}$ and is almost independent of the primary mass M_{WD} (Beuermann et al. 1998). We do not know M_{sec} , but we can estimate it using evolutionary models tabulated by Baraffe & Kolb (2000); these suggest that the secondary is between 0.23 and 0.56 M_{\odot} . At this P_{orb} , equation (1) of Beuermann et al. (1998) then implies $R_2 = 0.47 \pm 0.07 R_{\odot}$. Beuermann et al. (1999) tabulate absolute magnitudes and radii for late-type dwarfs as a function of spectral class, which implies a surface brightness for each star. In the range of spectral type we see here, these correspond to

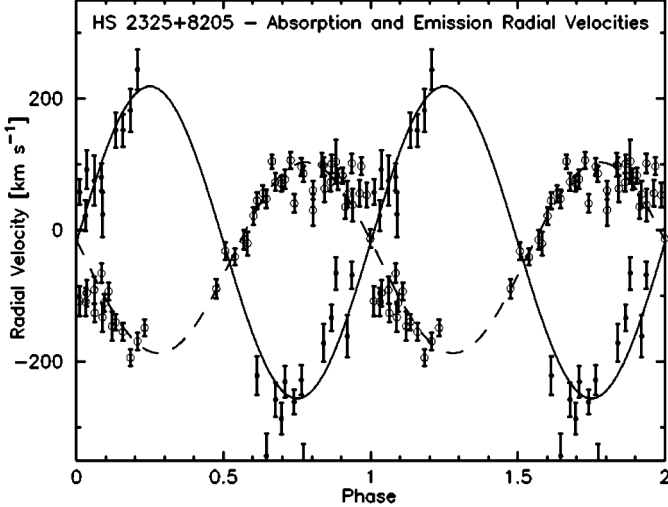


FIG. 4.—Radial velocities of HS 2325 in the quiescent state, plotted as a function of orbital phase. The open circles show the H α emission and their formal uncertainties, and the solid dots show the cross-correlation velocities of the M dwarf. There is a gap in coverage at $0.25 < \phi < 0.42$, and only some of the spectra yielded usable absorption velocities. The dashed curve shows the best fit to the emission velocities, with P_{orb} fixed, but with T_0 , K , and γ allowed to vary. For the absorption velocity fit (solid line), the T_0 was held fixed to the eclipse phase, and K and γ were adjusted.

$M_V = 8.8 \pm 0.7$ for a $1 R_\odot$ star, where the uncertainty includes both the spectral type uncertainty and the scatter among the tabulated points. Combining this with the radius yields an estimate of $M_V = 10.4 \pm 0.8$ for the secondary. The Galactic coordinates of HS 2325 are $(l, b) = (120^\circ, 20^\circ)$; at this location, Schlegel et al. (1998) estimate $E(B - V) = 0.19$ to the edge

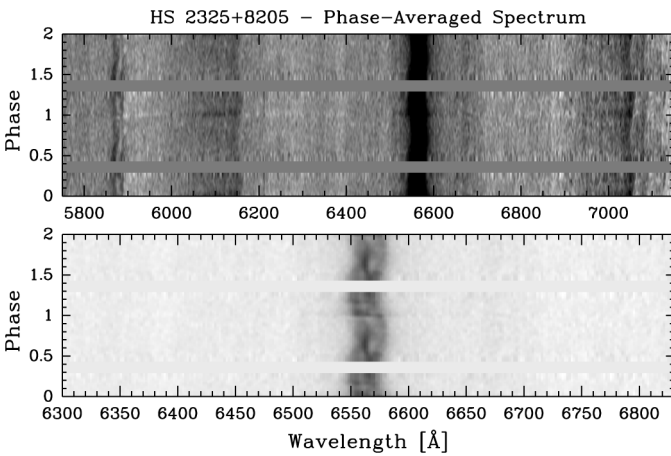


FIG. 5.—Grayscale representation of the low-state spectra, presented as a function of orbital phase. The data are repeated for a cycle to preserve continuity. The two panels show the same data, but differ in the choice of grayscale limits. The horizontal blank bars are holes in the phase coverage. To create the figure, the spectra were first rectified and cleaned of remaining cosmic ray hits; each line of the figure is a weighted average of spectra nearby in phase to the line's nominal phase, and the weights are computed using a narrow Gaussian.

of the Galaxy. Assuming that our object lies outside most of the dust, and taking the M dwarf contribution to the spectrum as $V = 19.0 \pm 0.4$, then yields an extinction-corrected distance modulus of $(m - M)_0 = 8.0 \pm 0.9$, corresponding to a distance of $400(+200, -140)$ pc. Note carefully that this estimate makes no assumption that the secondary follows a main-sequence mass-radius relation; it assumes only that the secondary's spectral type is a reliable guide to its surface brightness and that it fills its Roche lobe.

6. OUTBURST BEHAVIOR

We intensively monitored HS 2325 for about 50 days, starting from 2009 April 1 using small-aperture telescopes. Four outbursts have been recorded during this period, indicating a recurrence time of ~ 12 –14 days. Prominent in Figure 2 is a “long” outburst, lasting ~ 11 –12 days, followed by a seemingly “short” outburst. This could be a hint toward a bimodal distribution of the outburst duration, observed in many dwarf novae (see, e.g., Szkody & Mattei 1984; Ak et al. 2002). Further observations are required to establish a more accurate recurrence time and to check the consistency of the long and short outburst succession.

We have inspected version 7.12 (2009) of the Ritter & Kolb (R&K) catalog (Ritter & Kolb 2003) and compiled a list of UGem-type dwarf novae (UG) and Z Cam-type stars (ZC) that are found in the range of $4 \text{ hr} < P_{\text{orb}} < 5 \text{ hr}$. Only systems with confirmed UG/ZC status and with a quoted outburst recurrence period were considered. This left us with a list of 22 systems (out of the 39 listed in R&K in this P_{orb} range). In this list, ZC systems dominate the short end of the outburst recurrence period distribution (11–18 days), while UG systems tend to have longer intervals between outbursts (16–150 days). Our inferred outburst recurrence period places HS 2325 in the ZC region. However, as there has been no recorded standstill (the hallmark of ZC systems), its identification as either a UG or a ZC remains ambiguous.

7. ESTIMATES OF THE BINARY PROPERTIES

The standard treatment of eclipsing CVs (see, e.g., Wood et al. 1986, 1992; Littlefair et al. 2006a) involves the identification of the contact points of the white dwarf, the bright spot, and the accretion disk. The corresponding phase widths are then used to place firm (geometrical) constraints on the mass ratio q and the inclination angle i (e.g., Bailey 1979; Horne 1985) and to deduce information about the extent and location of the bright spot and the size of the accretion disk. Flickering can hinder attempts to identify the contact points. Averaging many light curves together is an often-applied solution (see, e.g., Copperwheat et al. [2010] for the case of IP Peg).

Although breaks in slope are seen in the light curve of HS 2325, the available data set is not of sufficient quality and time resolution to unambiguously identify the different

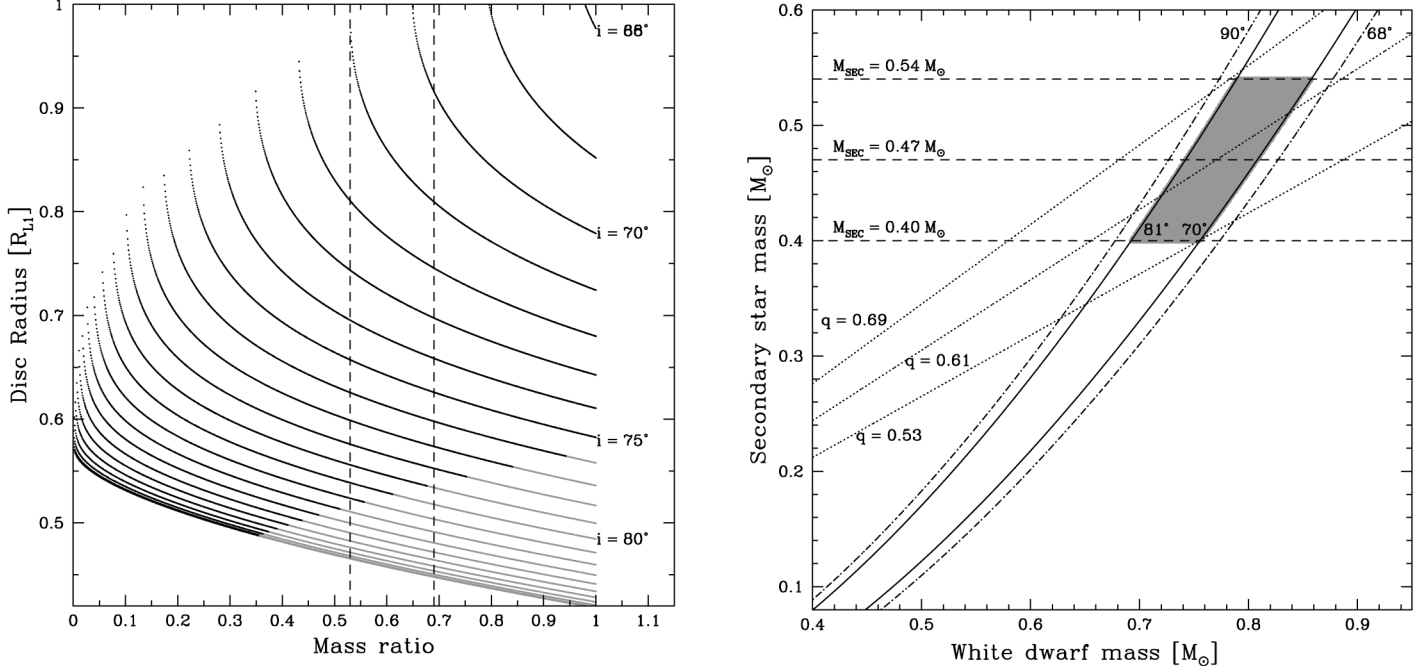


FIG. 6.—Left: Accretion disk radius in units of R_{L_1} as a function of q and i ; the curves are bound below (gray) by the requirement of a partial disk eclipse, and the vertical dashed lines correspond to a spectroscopic constraint on q (see text for details). Right: Constraints on the masses of the binary components; equation (2) plotted for $i = 68^\circ$, 90° (dash-dotted curves) and $i = 70^\circ$, 81° (solid curves), with constraints on the secondary mass assuming the mass-period relation of Smith & Dhillon (1998) (dashed lines) and constraints on the mass ratio q assuming $K_{\text{em}} = K_{\text{WD}}$ (dotted lines). Shaded in gray is the allowed parameter space, under the previous assumptions (see text for details).

contact points. Hence, the exact eclipse geometry of HS 2325 remains unclear.

In an attempt to constrain the parameter space (albeit roughly), we have to rely on theoretical predictions and empirical evidence from the observed CV population, coupled with the limited information that can be extracted from the light curves.

Following the procedure outlined in detail in Dhillon et al. (1991), the radius of the accretion disk can be determined as a function of the binary separation, q and i , for a given eclipse half-width at maximum intensity $\Delta\phi$ (essentially timing the first and last contacts of eclipse and dividing by two). $\Delta\phi$ was determined by eye to be $\Delta\phi = 0.1 \pm 0.02$. The large error is due to the fact that the exact beginning and end of the eclipse are uncertain because of flickering.

The left panel of Figure 6 shows the disk radius R_D (in units of the distance between the primary and the inner Lagrangian point, R_{L_1}) calculated using equations (3), (4), and (5) of Dhillon et al. (1991), for $0 \leq q \leq 1$ and various inclination angles. The curves are bound above by the requirement that $R_D \leq R_{L_1}$ and bound below by the requirement for a partial disk eclipse, satisfied if the disk radius is larger than the half-cord of the secondary (shown by the change in line color in the left panel of Fig. 6). This allows us to place a strict lower limit for the inclination angle to be $i_{\min} = 68^\circ$. However, the upper limit of i and the possible values of q remain unconstrained.

Using the mass function

$$f(M_{\text{WD}}) = \frac{(M_{\text{WD}} \sin i)^3}{(M_{\text{WD}} + M_{\text{sec}})^2} = \frac{P_{\text{orb}} K_{\text{sec}}^3}{2\pi G} \leq M_{\text{WD}}, \quad (2)$$

we can transform a given (q, i) pair to a unique $(M_{\text{WD}}, M_{\text{sec}})$ pair. The right panel of Figure 6 shows equation (2) calculated for $i_{\min} = 68^\circ$ and $i_{\max} = 90^\circ$, over a wide range in secondary mass, $0.1 \leq M_{\text{sec}}[M_{\odot}] \leq 0.6$. Allowed $(M_{\text{WD}}, M_{\text{sec}})$ pairs are located between the two dash-dotted curves.

We can further narrow down the parameter space by making two assumptions:

1. The secondary follows the mass-period relation of Smith & Dhillon (1998); their equation (8) (power-law fit) yields $M_{\text{sec}} = 0.43 \pm 0.07 M_{\odot}$, while their equation (9) (linear fit) yields $M_{\text{sec}} = 0.48 \pm 0.07 M_{\odot}$ (Fig. 6, right panel, dashed horizontal lines). An average of these values is in perfect agreement with the value of $M_{\text{sec}} = 0.45 M_{\odot}$ predicted by the revised model track of Knigge et al. (2011) for this orbital period.

2. The radial velocity variation of the emission lines tracks the motion of the white dwarf, so $K_{\text{em}} = K_{\text{WD}} = 145 \pm 9 \text{ km s}^{-1}$ and, therefore, $q = K_{\text{WD}}/K_{\text{sec}} = 0.61 \pm 0.08$ (Fig. 6, right panel, dotted lines).

While the latter is a frequently adopted assumption in CV research, it has to be viewed with a certain amount of caution (see, e.g., Shafter 1983 and Thorstensen 2000). An encouraging fact in the case of HS 2325 is that the phasing of the emission lines is consistent with the eclipse ephemeris. The constraint on q imposes a narrower range of inclination angles: $70^\circ \leq i \leq 81^\circ$ (Fig. 6, *left panel, dashed vertical lines*). If these assumptions are indeed correct, then the allowed (M_{WD} , M_{sec}) pairs are indicated as the gray shaded area in the right panel of Figure 6.

8. DISCUSSION AND CONCLUSIONS

In this article, we identified HS 2325 + 8205 as an eclipsing, frequently outbursting, dwarf nova above the CV orbital period gap and presented our photometric and spectroscopic data. We used these data to measure the orbital period and the radial velocity of the secondary star, as well as to provide initial estimates on the binary parameters. With the photometric data at hand, it remains unclear whether the white dwarf is fully eclipsed or not. The shallow eclipse depth could suggest that it is not eclipsed at all. High time resolution and signal-to-noise ratio data at quiescence are needed in order to unambiguously identify the eclipse geometry.

The short outburst cycle of \sim 12–14 days makes HS 2325 a plausible Z Cam-type candidate. If confirmed, it will be only the third known eclipsing Z Cam system, after EM Cyg (e.g., North et al. 2000 and references therein) and AY Psc (e.g., Gülsesen et al. 2009 and references therein).

HS 2325, with its high declination (circumpolar, ideal for observers in the northern hemisphere), short outburst recurrence

period, and magnitude range (accessible with 2–4 m class telescopes) offers an excellent target for systematic follow-up observations. Simultaneous high time resolution photometric and spectroscopic observations can provide unique insight in the changes in the structure of the accretion disk through techniques such as eclipse mapping (Horne 1985) and Doppler tomography (Marsh & Horne 1988).

Furthermore, the outbursts of HS 2325 can be picked up with relative ease by small-aperture telescopes, enabling the accumulation of a very long baseline of outburst data, which can then be compared with the predictions of the disk instability model. We strongly encourage observers from around the world to frequently monitor the system and put the Z Cam-type scenario to the test.

J. R. T. gratefully acknowledges support from the National Science Foundation, through grants AST-0307413 and AST-0708810. Based in part on observations made with the Nordic Optical Telescope, operated on the island of La Palma jointly by Denmark, Finland, Iceland, Norway, and Sweden, in the Spanish Observatorio del Roque de los Muchachos of the Instituto de Astrofísica de Canarias; on observations collected at the Centro Astronómico Hispano Alemán (CAHA) at Calar Alto, operated jointly by the Max-Planck Institut für Astronomie and the Instituto de Astrofísica de Andalucía (CSIC); on observations made at the 1.2 m telescope, located at Kryoneri Korinthias, and owned by the National Observatory of Athens, Greece; and on observations obtained at the MDM Observatory, operated by Dartmouth College, Columbia University, Ohio State University, and the University of Michigan.

REFERENCES

- Ak, T., Ozkan, M. T., & Mattei, J. A. 2002, *A&A*, 389, 478
 Aungwerojwit, A., et al. 2005, *A&A*, 443, 995
 Bailey, J. 1979, *MNRAS*, 187, 645
 Baraffe, I., & Kolb, U. 2000, *MNRAS*, 318, 354
 Bell, K. R., & Lin, D. N. C. 1994, *ApJ*, 427, 987
 Bertin, E., & Arnouts, S. 1996, *A&AS*, 117, 393
 Beuermann, K., Baraffe, I., & Hauschildt, P. 1999, *A&A*, 348, 524
 Beuermann, K., Baraffe, I., Kolb, U., & Weichhold, M. 1998, *A&A*, 339, 518
 Boeshaar, P. C. 1976, Ph.D. thesis, Ohio State Univ.
 Bruch, A. 2000, *A&A*, 359, 998
 Burderi, L., King, A. R., & Szuszkiewicz, E. 1998, *ApJ*, 509, 85
 Cannizzo, J. K. 1993, Accretion Disks in Compact Stellar Systems, ed. J. C. Wheeler (Singapore: World Scientific), 6
 Copperwheat, C. M., Marsh, T. R., Dhillon, V. S., Littlefair, S. P., Hickman, R., Gänsicke, B. T., & Southworth, J. 2010, *MNRAS*, 402, 1824
 Dhillon, V. S., Marsh, T. R., & Jones, D. H. P. 1991, *MNRAS*, 252, 342
 Dubus, G., Hameury, J.-M., & Lasota, J.-P. 2001, *A&A*, 373, 251
 Gänsicke, B. T., Araujo-Betancor, S., Hagen, H.-J., Harlaftis, E. T., Kitsionas, S., Dreizler, S., & Engels, D. 2004, *A&A*, 418, 265
 Gülsesen, H., Retter, A., Liu, A., & Esenoglu, H. 2009, *NewA*, 14, 330
 Hagen, H.-J., Groote, D., Engels, D., & Reimers, D. 1995, *A&AS*, 111, 195
 Horne, K. 1985, *MNRAS*, 213, 129
 ———. 1986, *PASP*, 98, 609
 Knigge, C., Baraffe, I., & Patterson, J. 2011, *ApJS*, 194, 28
 Krzeminski, W. 1965, *ApJ*, 142, 1051
 Kurtz, M. J., & Mink, D. J. 1998, *PASP*, 110, 934
 Lasota, J.-P. 2001, *NewA Rev.*, 45, 449
 Littlefair, S. P., Dhillon, V. S., Marsh, T. R., & Gänsicke, B. T. 2006a, *MNRAS*, 371, 1435
 Littlefair, S. P., Dhillon, V. S., Marsh, T. R., Gänsicke, B. T., Southworth, J., & Watson, C. A. 2006b, *Science*, 314, 1578
 Marcy, G. W., Lindsay, V., & Wilson, K. 1987, *PASP*, 99, 490
 Marsh, T. R., & Horne, K. 1988, *MNRAS*, 235, 269
 Morgenroth, O. 1936, *Astron. Nachr.*, 258, 265
 North, R. C., Marsh, T. R., Moran, C. K. J., Kolb, U., Smith, R. C., & Stehle, R. 2000, *MNRAS*, 313, 383
 Osaki, Y. 1996, *PASP*, 108, 39
 Ritter, H., & Kolb, U. 2003, *A&A*, 404, 301
 Schlegel, D. J., Finkbeiner, D. P., & Davis, M. 1998, *ApJ*, 500, 525
 Schneider, D. P., & Young, P. 1980, *ApJ*, 238, 946
 Shafter, A. W. 1983, *ApJ*, 267, 222
 ———. 1992, *ApJ*, 394, 268

- Smak, J. 1984, PASP, 96, 5
- Smith, D. A., & Dhillon, V. S. 1998, MNRAS, 301, 767
- Southworth, J., Hickman, R. D. G., Marsh, T. R., Rebassa-Mansergas, A., Gänsicke, B. T., Copperwheat, C. M., & Rodríguez-Gil, P. 2009, A&A, 507, 929
- Szkody, P., & Mattei, J. A. 1984, PASP, 96, 988
- Thorstensen, J. R. 2000, PASP, 112, 1269
- Warner, B. 1995, Cataclysmic Variable Stars (Cambridge: Cambridge Univ. Press)
- Wood, J. H., Horne, K., Berriman, G., & Wade, R. A. 1989, ApJ, 341, 974
- Wood, J., Horne, K., Berriman, G., Wade, R., O'Donoghue, D., & Warner, B. 1986, MNRAS, 219, 629
- Wood, J. H., Horne, K., & Vennes, S. 1992, ApJ, 385, 294